RESEARCH ARTICLE
ATMOSPHERIC PHYSICS

Earth and Planetary Physics
9: 69–80, 2025
doi: 10.26464/epp2024033

Vertical gradients of neutral winds observed by ICON and estimated by the Horizontal Wind Model during the geomagnetic storm on August 26–28, 2021

JiaWei Wu, Chao Xiong*, YuYang Huang, and YunLiang Zhou

Department of Space Physics, School of Electronic Information, Hubei Luojia Laboratory, Wuhan University, Wuhan 430072, China

Key Points:

- Horizontal neutral wind estimations from Horizontal Wind Model 14 (HWM14) show generally good agreement with the observations from the Ionospheric Connection Explorer (ICON) during geomagnetic quiet periods.
- Horizontal winds observed by ICON show different vertical shear structures at different stages of a geomagnetic storm.
- The HWM14 was insufficient to accurately estimate the vertical shear structures of horizontal winds during the geomagnetic storm.

Citation: Wu, J. W., Xiong, C., Huang, Y. Y., and Zhou, Y. L. (2025). Vertical gradients of neutral winds observed by ICON and estimated by the Horizontal Wind Model during the geomagnetic storm on August 26–28, 2021. *Earth Planet. Phys.*, *9*(1), 69–80. http://doi.org/10.26464/epp2024033

Abstract: The Michelson Interferometer for Global High-resolution Thermospheric Imaging (MIGHTI) onboard the Ionospheric Connection Explorer (ICON) satellite offers the opportunity to investigate the altitude profile of thermospheric winds. In this study, we used the red-line measurements of MIGHTI to compare with the results estimated by Horizontal Wind Model 14 (HWM14). The data selected included both the geomagnetic quiet period (December 2019 to August 2022) and the geomagnetic storm on August 26–28, 2021. During the geomagnetic quiet period, the estimations of neutral winds from HWM14 showed relatively good agreement with the observations from ICON. According to the ICON observations, near the equator, zonal winds reverse from westward to eastward at around 06:00 local time (LT) at higher altitudes, and the stronger westward winds appear at later LTs at lower altitudes. At around 16:00 LT, eastward winds at 300 km reverse to westward, and vertical gradients of zonal winds similar to those at sunrise hours can be observed. In the middle latitudes, zonal winds reverse about 2–4 h earlier. Meridional winds vary more significantly than zonal winds with seasonal and latitudinal variations. According to the ICON observations, in the northern low latitudes, vertical reversals of meridional winds are found at 08:00–13:00 LT from 300 to 160 km and at around 18:00 LT from 300 to 200 km during the June solstice. Similar reversals of meridional winds are found at 04:00–07:00 LT from 300 to 160 km and at 22:00–02:00 LT from 270 to 200 km during the December solstice. In the southern low latitudes, meridional wind reversals occur at 08:00–11:00 LT from 200 to 160 km and at 21:00–02:00 LT from 300 to 200 km during the June solstice. During the December solstice, reversals of the meridional wind appear at 20:00–01:00 LT below 200 km and at 06:00–11:00 LT from 300 to 160 km. In the northern middle latitudes, the northward winds are dominant at 08:00–14:00 LT at 230 km during the June solstice. Northward winds persist until 16:00 LT at 160 and 300 km. During the December solstice, the northward winds are dominant from 06:00 to 21:00 LT. The vertical variations in neutral winds during the geomagnetic storm on August 26–28 were analyzed in detail. Both meridional and zonal winds during the active geomagnetic period observed by ICON show distinguishable vertical shear structures at different stages of the storm. On the dayside, during the main phase, the peak velocities of westward winds extend from a higher altitude to a lower altitude, whereas during the recovery phase, the peak velocities of the westward winds extend from lower altitudes to higher altitudes. The velocities of the southward winds are stronger at lower altitudes during the storm. These vertical structures of horizontal winds during the storm could not be reproduced by the HWM14 wind estimations, and the overall response to the storm of the horizontal winds in the low and middle latitudes is underestimated by HWM14. The ICON observations provide a good dataset for improving the HWM wind estimations in the middle and upper atmosphere, especially the vertical variations.

Keywords: horizontal neutral winds; vertical gradients; Ionospheric Connection Explorer satellite; Horizontal Wind Model 14; geomagnetic storm

First author: J. W. Wu, 1610338119@qq.com
Correspondence to: C. Xiong, xiongchao@whu.edu.cn
Received 14 DEC 2023; Accepted 24 APR 2024.
First Published online 08 AUG 2024.

1. Introduction

The atmospheric neutral winds play an important role in the dynamic evolution of Earth's ionosphere at the low and middle latitudes, such as pushing ions and electrons across the magnetic field lines and generating the dynamo electric fields (e.g., Heelis,

2004; Richmond, 2011). During geomagnetic quiet periods, both the day–night difference in heating caused by solar radiation and the upward-propagating atmospheric tides can affect the distribution of global thermospheric winds. In contrast, during geomagnetic disturbed periods, two main sources can cause additional disturbances to the neutral winds: (1) the collisional interaction with rapidly convecting ions driven by strong electric fields, and (2) the Joule heating attributable to strong high-latitude electric currents (Richmond et al., 2003). The neutral winds have frequently been observed to change substantially compared with their quiet-time patterns. Thus, understanding the respective characteristics of neutral winds during both geomagnetic quiet and disturbed periods is important for studying and estimating the evolutionary structure of the upper atmosphere and ionosphere.

Over the past few decades, ground-based and satellite measurements, as well as model estimations, have been used to investigate the characteristics of neutral winds in the upper atmosphere. In general, horizontal winds show typical diurnal variations during geomagnetic quiet periods. Antoniadis (1976) mentioned that the meridional winds during equinoxes and the December solstice are poleward from 06:00 to 20:00 local time (LT), whereas they are poleward from 09:00 to 13:00 LT during the June solstice. Lieberman et al. (2013) reported that the westward wind was observed by the CHAllenging Minisatellite Payload (CHAMP) between 03:00 and 14:00 LT, with the eastward wind prevailing during the remaining hours. In addition to the diurnal variation, Liu HX et al. (2006) reported that the solar flux can significantly influence the zonal wind in both the daytime and nighttime. Emmert et al. (2001) found, based on measurements of the Wind Imaging Interferometer (WINDII) instrument onboard the Upper Atmosphere Research Satellite (UARS), that during geomagnetic storms, the disturbance zonal and meridional winds are mainly westward and equatorward, respectively. Further, Xiong C et al. (2015) found, by applying a superposed epoch analysis to the zonal winds measured by the CHAMP satellite, that the westward disturbance wind is first observed in the subauroral latitudes, and then it reaches the low and equatorial regions in approximately 3–4 h. Disturbance winds further cause perturbations of the equatorial electrojet and zonal electric field at the equatorial region, showing the most prominent effects from midnight to the dawn hours (Xiong C et al., 2016).

Although quite good progress has been made in investigating the horizontal winds of the upper atmosphere, very few studies have focused on the vertical structures of the neutral winds. One possible reason is the lack of observations. However, as introduced above, the neutral winds are involved in various physical and chemical processes in the thermosphere, and they transfer energy between atmospheric waves at different altitudes; thus, the vertical structure of neutral winds should play an important role in the ionospheric electrodynamics. The WINDII instrument of the UARS mission was the first to measure the winds at different altitudes. McLandress et al. (1994) used the meridional wind from WINDII during March and April 1993 to investigate the thermospheric tidal signatures at different altitudes. They showed the meridional wind profiles of the corresponding period to be a function of height and LT. They found that at 20°N, the propagating diurnal tide was clearly visible but that it was without clear vertical variations above 120 km. Fesen (1997) reported that the meridional wind perturbations caused by geomagnetic storms could penetrate down to approximately 100 km, depending on the LT and season. On the basis of results from the Coupled Magnetosphere–Ionosphere–Thermosphere (CMIT) model, Wang W et al. (2008) showed that noticeable vertical shear occurred globally during a geomagnetic storm and that such vertical wind shear was almost absent during quiet periods, except in a few cases at low and middle latitudes. Harding et al. (2017a) analyzed the observations from the North American Thermosphere–Ionosphere Observing Network (NATION) over a period of 5 years (2011–2016). They found that the horizontal winds showed quite prominent altitude dependences in the middle latitudes during a geomagnetic storm.

Recently, the launch of the Ionospheric Connection Explorer (ICON) satellite has made it possible to measure the horizontal neutral winds in the altitude range from 90 to 300 km, based on the Global High-Resolution Thermospheric Imaging (MIGHTI) instrument onboard. The neutral wind measurements from MIGHTI have been validated against other observations and model estimations. Makela et al. (2021) compared the red-line data of MIGHTI on ICON with those from two ground-based Fabry–Perot interferometers (FPIs) located in Urbana, Illinois, USA (40.2°N, 88.2°W) and Marrakesh, Morocco (31.2°N, 7.9°W). They found good agreement between observations from ICON and the FPIs, with mean differences of less than 11 m/s in magnitude. Harding et al. (2021) further compared neutral wind observations at different altitudes made by ICON and four ground-based specular meteor radars. They reported consistent wind measurements between ICON and the radars, which showed an average discrepancy of 4.5 m/s. McGinness et al. (2023) focused on a minor geomagnetic storm and found that the horizontal meridional winds at 223 km changed dramatically, whereas they observed no westward perturbation in the low–middle latitudes. Huang YY et al. (2023) analyzed the neutral wind measurements of ICON over a 2-year period and found that vertical gradients of horizontal winds were in the low F region and were sometimes observed during geomagnetic quiet periods. One pending question is whether such vertical gradients of horizontal winds also exist during geomagnetic storms.

In this study, we focus on the vertical structure of horizontal winds during the geomagnetic storm on August 26–28, 2021. The measurements from the MIGHTI instrument onboard ICON between 160 and 300 km are compared with the results from the 2014 Horizontal Wind Model (HWM14), the most often used empirical model of horizontal winds for the upper atmosphere. To emphasize the vertical structure of horizontal winds caused by the geomagnetic storm, we also provide a comparison between ICON and HWM14 during magnetic quiet periods. This article follows the conventional structure. In Section 2, we provide a short introduction to the MIGHTI wind measurements from ICON and the HWM14 estimations. In Section 3, we present altitude profiles of the horizontal winds from ICON and HWM14 during both geomagnetic quiet and disturbed periods. In Section 4, we

provide a discussion in relation to earlier studies. In Section 5, we summarize the main findings of this study.

2. Dataset Description

2.1 Horizontal Wind Measurements from MIGHTI/ICON

The National Aeronautics and Space Administration's (NASA's) ICON satellite was launched on October 10, 2019, with an inclination of 27° and an initial altitude of 590 km. It takes approximately 24 days for ICON to cover all 24 LT hours. For the horizontal winds, the MIGHTI instrument uses the Doppler Asymmetric Spatial Heterodyne (DASH) technique (Englert et al., 2007, 2017) to measure the middle and upper atmospheric wind field. This technique can calculate the atmospheric wind speed by measuring the Doppler frequency shift by detecting the phase shift of the airglow spectral line. The MIGHTI instrument measures the Doppler shift of emission lines from oxygen on green (557.7 nm) and red (630.0 nm). Thus, wind data provided by the MIGHTI instrument on ICON are available in both the red and green channels, with a time resolution of 30 s. The red-line data cover the altitude range from 160 to 300 km in the day and from 200 to 300 km at night, with a step of 10 km, whereas the green-line data cover altitudes from 90 to 220 km in the day and from 90 to 105 km at night, with a step of 3 km. Note that the MIGHTI instrument measures winds at the E region footprint of the magnetic field line reaching the ICON orbit, which is different from the *in situ* ion density and plasma drift measured by ICON along its orbit. A detailed projection of MIGHTI measured winds and the ICON orbit was provided by Immel et al. (2021).

To check the neutral winds during quiet and storm periods, as much wind data as possible for each LT and altitude are needed. We first attempt to integrate the red- and green-line data from MIGHTI. However, the combined winds from the two channels are not comparable with each other because they cover different LTs and have different altitude resolutions. Because of the narrowing of the atmospheric emission profiles, MIGHTI can hardly measure neutral winds above an altitude of 105 km at night from the green line (Harding et al., 2017b). The ability of ICON to detect neutral wind fields below 200 km changes at around 06:00 and 18:00 LT; therefore, green-line data above 105 km are available only during the day, from 06:00 to 18:00 LT. Note that clear errors in the wind retrievals occur when either of MIGHTI's lines of sight cross the day–night boundary or are at the edge of the equatorial ionization anomaly, as pointed out by Harding et al. (2017b). Therefore, one should be cautious when using the MIGHTI measurements around sunrise and sunset. For the above-mentioned reasons, in this study we finally choose the wind data of the red channel from December 2019 to August 2022, with the latest data version of 05.

2.2 HWM14

The HWM14 is the latest model available for estimating the horizontal winds in the middle and upper atmosphere. The HWM07 was updated with additional data from the ground-based 630-nm FPI measurements in the equatorial and polar regions, as well as cross-track winds from the Gravity Field and Steady State Ocean Circulation Explorer (GOCE) satellite (Drob et al., 2015). The HWM14 provides the horizontal winds as a function of latitude, longitude, altitude, day of the year, and universal time (UT) of a day. Drob et al. (2015) reported that empirical winds from HWM14 are more self-consistent with the climatological ionosphere plasma distribution and electric field patterns than were prior versions of the HWM model. To perform a better comparison, we use the UT and location of the ICON wind data as inputs for wind estimations from HWM14.

3. Results

3.1 Horizontal Wind Distributions During Quiet Time

As introduced in Section 1, to highlight the vertical structure of horizontal winds caused by the geomagnetic storm, we first provide a detailed comparison of the horizontal winds between ICON and HWM14 during magnetic quiet periods. These data are divided into three seasons: equinoxes (including March, April, September, and October), the June solstice (including May, June, July, and August), and the December solstice (including January, February, November, and December). Because the neutral wind data from ICON cover only latitudes between −12°N and 42°N geographic latitude (Glat), we therefore divide the data into three latitude regions: southern low latitudes (−15°N to 0°N Glat), northern low latitudes (0°N to 15°N Glat), and northern middle latitudes (15°N to 45°N Glat).

For each season and Glat bin, the zonal wind estimations from HWM14 and the measurements from ICON are divided into altitude versus LT bins. The bin size for altitude is 10 km and the LT is 0.1 h. The averaged values of zonal winds at different altitudes and LTs are shown in Figure 1 for HWM14 (left) and ICON (right), separately for the three seasons and latitude regions. The negative and positive zonal winds direct to the westward and eastward, respectively.

As shown in Figure 1, for HWM14, zonal winds show prominent diurnal variation, and such diurnal variation is less dependent on season. In both the northern and southern low latitudes (Figures 1a and 1b), zonal winds above 230 km are westward from 06:00 to 16:00 LT, whereas they change to eastward for the rest of the LT hours. At around sunrise hours, the westward winds appear at later LTs at lower altitudes. Similar vertical gradients of zonal winds exist at around 16:00 LT. In the northern middle latitude region from 15°N to 45°N Glat (Figure 1c), the situation is slightly different in that the changes in zonal wind direction appear earlier than those at low latitudes, and they show clear seasonal differences. For example, the zonal winds reverse from eastward to westward at 02:00 LT. They appear approximately 1 h earlier than those during the equinoxes and 2 h earlier than those during the December solstice. The northern middle latitude zonal winds also reverse from westward to eastward at 16:00 LT during the June solstice, appearing approximately 1 h later than those during the equinoxes and 2 h later than those during the December solstice. Vertical gradients can also be clearly observed when the zonal winds reverse.

The diurnal variation of the zonal winds, westward between around 06:00 and 16:00 LT and eastward during the rest of the LT hours in the low latitudes, and the changes in the zonal wind direction, appearing earlier in the northern middle latitudes as observed by ICON during all three seasons and in three latitude regions, show altitude and LT distributions generally consistent

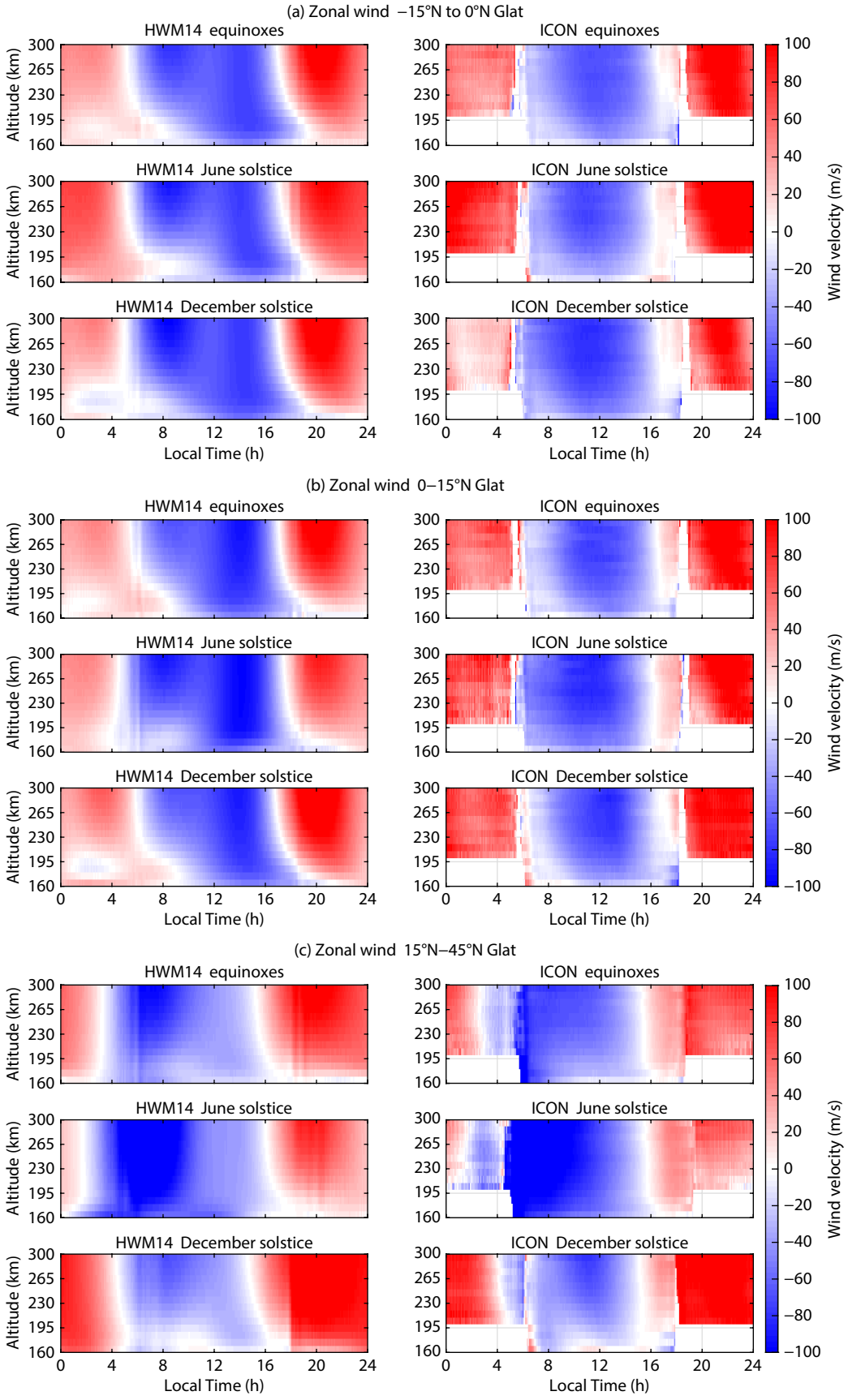

Figure 1. Averaged zonal winds at (a) −15°N to 0°N, (b) 0°N to 15°N, (c) 15°N to 45°N from HWM14 (left) and ICON (right) in different seasons — (top) equinoxes, (middle) June solstice, and (bottom) December solstice — as a function of the altitude and local time. The positive and negative values represent the eastward and westward winds, respectively.

with those from the HWM14 estimations. Another common feature between the observations and model estimations is that around sunrise hours, the westward zonal winds gradually diminish as the altitude decreases; in other words, the westward winds appear at a later LT at a lower altitude, especially for the northern and southern low latitudes (Figures 1a and 1b). Similar vertical reversals of zonal winds occur at around 16:00 LT. Such a feature reveals that around sunrise, clear vertical gradients of the zonal winds exist in the altitude range of 160 to 300 km.

Although the zonal winds between the observations and model estimations are similar, differences can still be found between them. For example, in the northern and southern low latitude regions, the intensity of nighttime eastward winds is slightly larger from ICON observations than from HWM14 estimations, except in the southern low latitude during the December solstice (bottom panel of Figure 1a). In contrast, in the northern middle latitude region, the ICON satellite observed slightly weaker nighttime eastward winds during all three seasons. As mentioned in Section 2, clear errors in the wind retrievals occur when the MIGHTI lines of sight cross the day–night boundary. This leads to data gaps around 06:00 and 18:00 LT, or it makes the amplitude change rather large around these two LT sectors. This feature is particularly pronounced in the northern middle latitude region, which can be seen in both the ICON observations and the HWM14 estimations.

Figure 2 shows the variations in diurnally averaged meridional winds (positive northward) under the same classification conditions as Figure 1. Compared with the zonal winds, the meridional winds show greater seasonal and latitude dependence.

For HWM14, the variations in diurnally averaged meridional winds are different in the northern and southern low latitudes. During the equinoxes, the HWM14 estimations show that in the southern low latitudes (top panel of Figure 2a), the northward winds are dominant between 00:00 and 06:00 LT, and then gradually reverse to southward. After 13:00 LT, the southward winds turn back northward again. In the northern low latitudes (top panel of Figure 2b), the meridional winds are mainly northward, but at 20:00 LT and 00:30 LT, the meridional winds at 300 km gradually reverse from northward to southward and from southward to northward, respectively, and they show reduced amplitude with decreasing altitude at later LT hours. In addition, weak, short-lived southward winds are observed at approximately 190 to 210 km from 08:00 to 10:00 LT and at approximately 160 km from 16:00 to 20:00 LT. During the June solstice, in the southern low latitudes (middle panels of Figure 2a), weak northward winds dominate from 03:00 to 06:00 LT, and at other LT hours, the northward winds reverse to southward and become stronger. Between 0°N and 15°N latitude (middle panel of Figure 2b), the HWM14 estimations show that the meridional winds are mainly southward. However, the southward winds reverse to northward from 160 km at 06:00 LT to 230 km at 09:00 LT, and the northward winds then reverse back to southward from 230 km at 09:00 LT to 160 km at 13:00 LT. After 16:00 LT, weak northward winds develop at 300 km and gradually extend to the lower altitudes. During the December solstice, the HWM14 estimations show that in the southern low latitude (bottom panel of Figure 2a), the meridional winds are mainly northward, with northward winds reversing to southward from 160 km at 06:00 LT to 300 km at 09:00 LT and then back to northward from 300 km at 09:00 LT to 160 km at 12:00 LT. In the northern low latitude (bottom panel of Figure 2b), the southward winds are visible for a few hours around 00:00 and 08:00 LT, roughly in the 170- to 200-km altitude range. Comparatively, the meridional winds in the northern middle latitudes (bottom panels of Figure 2c) show more prominent diurnal variation than those in the low latitude region. During the equinoxes, the meridional winds are mainly southward at 05:00 and 20:00 LT and are northward at the other times. During the June solstice, the northward winds are dominant from 08:00 to 13:00 LT, whereas at the rest of the LT hours, the southward winds are dominant. During the December solstice, the meridional winds are mainly southward at 04:00 and 21:00 LT and northward at the other times. Clear vertical gradients of the meridional winds can be observed when reversals of the meridional winds appear.

In general, the meridional wind estimations from HWM14 and the ICON observations are in relatively good agreement. For example, meridional winds from both the ICON observations and the HWM14 estimations show that near the equator (Figures 2a and 2b), southward winds dominate during the June solstice and northward winds dominate during the December solstice. In the northern middle latitude (Figure 2c), northward winds prevail much longer and with stronger amplitudes when they are approaching the December solstice. In the northern low latitude, the meridional winds during the June solstice (middle panels of Figure 2b) are stronger at lower altitudes in the daytime and at higher altitudes at nighttime. In addition, clear vertical gradients of the meridional winds exist in the altitude range from 160 to 300 km in the morning, especially in the low latitudes (Figure 2a and 2b).

However, some differences also exist between the observations and model estimations of the meridional winds. The variations in their intensity at different altitudes are sometimes different. For example, during the equinoxes in the southern low latitudes (top panels of Figure 2a), the meridional winds observed by ICON are usually faster at higher altitudes (above 230 km), whereas in the HWM estimations, the meridional winds at lower altitudes (below 230 km) are faster. Additionally, reversals of the meridional winds are different between the ICON observations and HWM estimations. For example, according to the ICON observations, in the northern low latitudes (Figure 2b), vertical reversals of the meridional winds are found at 08:00–13:00 LT from 300 to 160 km and at around 18:00 LT from 300 to 200 km during the June solstice. Similar reversals of the meridional winds are also found at 04:00–07:00 LT from 300 to 160 km and at 22:00–02:00 LT from 270 to 200 km during the December solstice. In the southern low latitudes (Figure 2a), meridional wind reversals occur at 08:00–11:00 LT from 200 to 160 km and at 21:00–02:00 LT from 300 to 200 km during the June solstice. During the December solstice, reversals of the meridional winds appear at 20:00–01:00 LT below 200 km and at 06:00–11:00 LT from 300 to 160 km during the December solstice. In the northern middle latitudes (Figure 2c), the northward winds are dominant from 08:00 to 14:00 LT at 230 km during the June solstice, and the northward winds persist until 16:00 LT at 160 and 300 km. During the Decem-

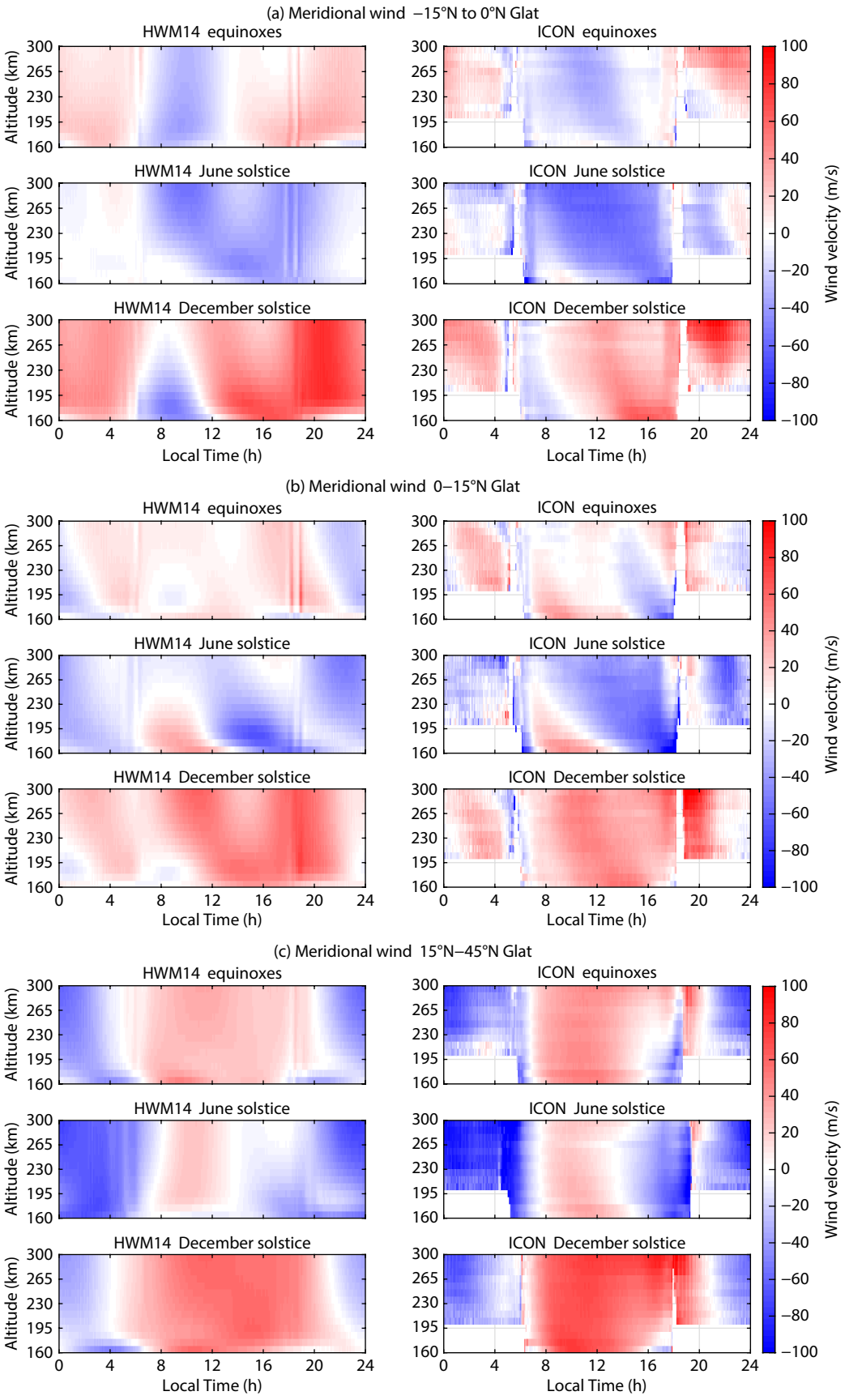

Figure 2. Same as Figure 1, but for meridional winds. The positive and negative values represent the northward and southward winds, respectively.

ber solstice, the northward winds are dominant from 06:00 to 21:00 LT, whereas the southward winds are dominant at the other times. In the northern middle latitudes (top and middle panels of Figure 2c), the observations from ICON show an unusual wind direction reversal during the equinoxes and at dusk during the June solstice. Several hours before 18:00 LT, the meridional winds are southward, but after 18:00 LT, they begin to reverse to northward.

3.2 Horizontal Wind Distributions During the Geomagnetic Storm on August 26–28, 2021

After investigating the characteristics of the horizontal winds during geomagnetic quiet periods, we turn our attention to the response of horizontal winds during the geomagnetic storm. After checking all the storms that occurred during the ICON mission period, we find that the horizontal winds show the most prominent altitude gradients during the storm that occurred on August 26–28, 2021. Therefore, in the rest of this section, we show the ICON observations as well as the HWM14 estimations during this storm.

Figure 3 shows the variations in solar wind velocity (V_{sw}) at the Earth's bow shock, the three components of the interplanetary magnetic field (IMF) in the Geocentric Solar Magnetospheric (GSM) coordinate system, and the SYM-*H* index on August 26–28, 2021. Around 01:00 UT on August 27 (indicated by the vertical dotted line), sudden increases in the V_{sw} and SYM-*H* index were observed, which indicates a sudden storm commencement (SSC). Afterward, the IMF shows relatively large variations. Around 14:00 UT on August 27, the IMF B_z suddenly turns southward and the SYM-*H* index gradually drops, indicating the main phase of the storm. Around 00:30 UT on August 28, the SYM-*H* index reaches its minimum of approximately −89 nT, which indicates that the storm has evolved from the main phase to the recovery phase.

Figure 4 shows a comparison of an orbit that records the wind profile by ICON and HWM14 on August 26, 2021, the day before the storm. Figures 4c–4f are zonal and meridional wind profiles plotted by using the HWM14 and ICON results. Figures 4a and 4b, respectively, show the *ap* index and the SYM-*H* index corresponding to the neutral winds from HWM14 and ICON, whereas Figures 4g and 4h depict the latitude, longitude, and LT of each UT in the orbit. Because the latitudes and LTs observed by ICON in different orbits change little over several days, we can further explore the wind changes at different stages of this storm based on Figure 4. To better compare the results of ICON and HWM14 within the same range, the wind amplitudes from HWM14 in Figure 4 and all subsequent figures are multiplied by a factor of 2. From Figure 4, we can see that in the results from ICON and HWM14, the direction of the zonal winds (Figures 4c and 4d) is generally consistent. As for the meridional winds, the HWM14 estimations (Figure 4e) show that between 9.4 and 9.6 UT, at a latitude above 35°N, below an altitude of 200 km, the meridional winds are mainly southward, and in the altitude range of 200 to 300 km, they turn northward and gradually become stronger with the increase in altitude. However, in the ICON observations (Figure 4f), no wind reversal occurs in the vertical direction in the same region. This difference is consistent with previous statistical results based on neutral winds during the geomagnetic quiet-period data in Section 3.1.

Figure 5 shows a typical orbit on August 27, 2021, which records the shear in the main phase of this storm. In the observation of a single orbit, the propagation process of disturbance from middle latitudes to low latitudes is visible. According to the observations by ICON, compared with the neutral winds before the storm in Figure 4, we find that the daytime westward winds strengthen at higher altitudes and the nighttime eastward winds are reduced at lower altitudes (Figure 5d), which indicates that the disturbance in zonal winds is westward. In the northern hemisphere, between 19.0 and 19.2 UT, the daytime westward winds are stronger at higher altitudes. From 19.2 to 19.3 UT, westward winds are greater than 200 m/s at almost all altitudes, and afterward, the westward zonal winds at the northern middle latitudes gradually diminish with decreases in altitude. Between 19.9 and 20.1 UT, the amplitudes of nighttime eastward winds at southern low latitudes

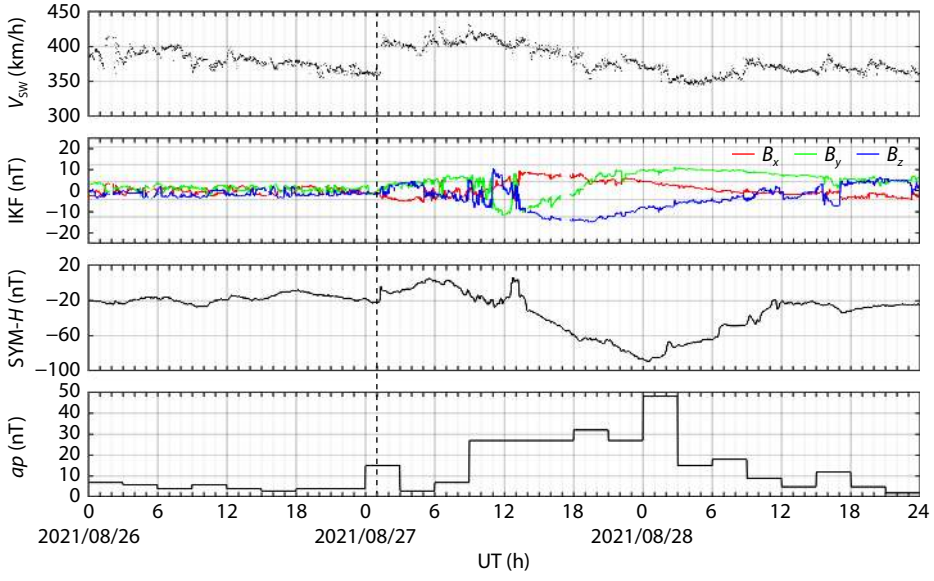

Figure 3. Temporal variations of V_{SW}, IMF, SYM-*H*, and *ap* index during August 26–28, 2021.

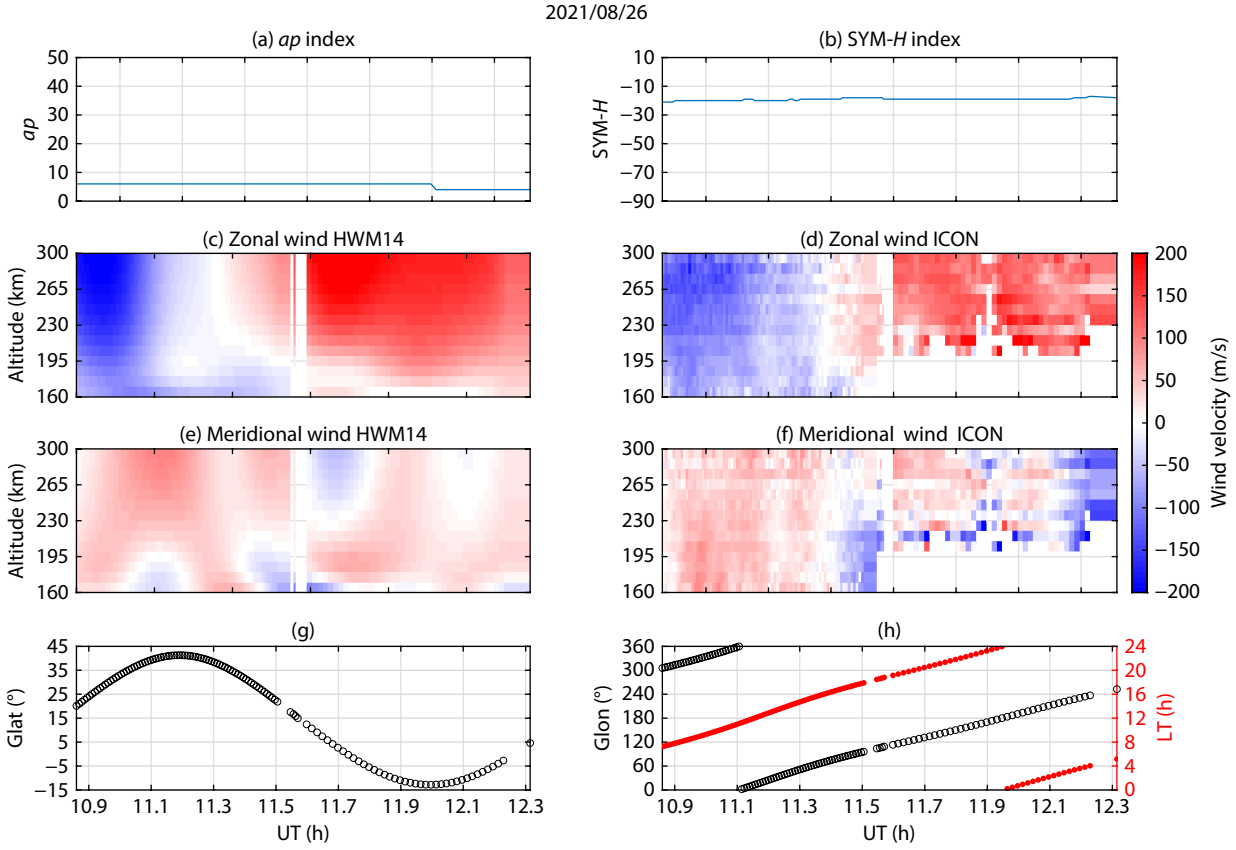

Figure 4. Zonal (the second line) and meridional wind (the third line) from HWM14 (left) and ICON (right) profile of a single typical orbit before the storm. Panels (a) and (b), respectively, depict the ap index and SYM-*H* index corresponding to the neutral winds from HWM14 and ICON. Panels (g) and (h), respectively, depict the latitude, longitude, and local time of each universal time in the orbit.

decrease and even reverse to westward below 230 km. Meanwhile, both the daytime and the nighttime meridional winds are mainly strengthened in a southwardly direction (Figure 5f); in other words, the disturbance in meridional winds is mainly southward. In the northern latitudes, ICON observed stronger southward winds at lower altitudes between 19.0 and 19.8 UT. In the southern hemisphere (between 19.9 and 20.3 UT), nighttime meridional winds above 250 km are mainly southward. Additionally, the responses of both zonal and meridional winds in the middle latitudes in the main phase are stronger than those in the low latitudes.

According to the wind estimations of HWM14 during the main phase of the storm, from 19.0 to 19.6 UT on August 27, 2021 (Figure 5c), the estimated zonal winds are westward at almost all altitudes, with stronger values at higher altitudes from 19.0 to 19.3 UT and at lower altitudes from 19.3 to 19.6 UT. From 19.6 to 20.4 UT, the eastward winds at lower altitudes reverse to westward, similar to the observations from ICON, but those at higher altitudes do not weaken as obviously as in the ICON observations. At the same time, the wind estimations from HWM14 (Figure 5e) underestimate the response of meridional winds during the main phase of the storm because the variations in the meridional winds are much weaker than those in the observations from ICON. Considering that the wind amplitudes from HWM14 in Figure 5 are multiplied by a factor of 2, the response of zonal winds during the main phase of the storm is actually also underestimated by HWM14.

The daytime zonal winds from ICON show noticeably clear vertical shears from the altitude profile, as shown in Figure 5d, extending from 300 km at 19.3 UT (around 42°N Glat, 255°E Glon) to 160 km at 19.5 UT (around 33°N Glat, 300°E Glon). This shear structure occurs during the main phase of the storm and by approximately 18 h after the SSC, with the SYM-*H* index decreasing and the IMF B_z reaching approximately −14 nT. Compared with the winds during geomagnetic quiet periods (as shown in the middle panels of Figure 1c), we consider that this vertical shear structure is mainly caused by the geomagnetic storm. However, this vertical shear structure failed to be reproduced by the wind estimations from HWM14 (Figure 5c), which could be because the wind estimations during an active magnetic period were superimposed on only the quiet winds, with no vertical gradient disturbance winds.

During the recovery phase of this storm on August 28, 2021, the response of the winds becomes different, as shown in Figure 6. The response of the zonal winds is more obvious than that of the meridional winds. According to the ICON observations, from 4.6 to 4.9 UT, zonal winds in the northern hemisphere increase westwardly compared with before the storm, whereas from 5.0 to 5.6 UT, zonal winds change little compared with before the storm. From 4.6 to 4.7 UT and also after 5.1 UT, the meridional winds (Figure 6f) at relative higher altitudes are northward and those at

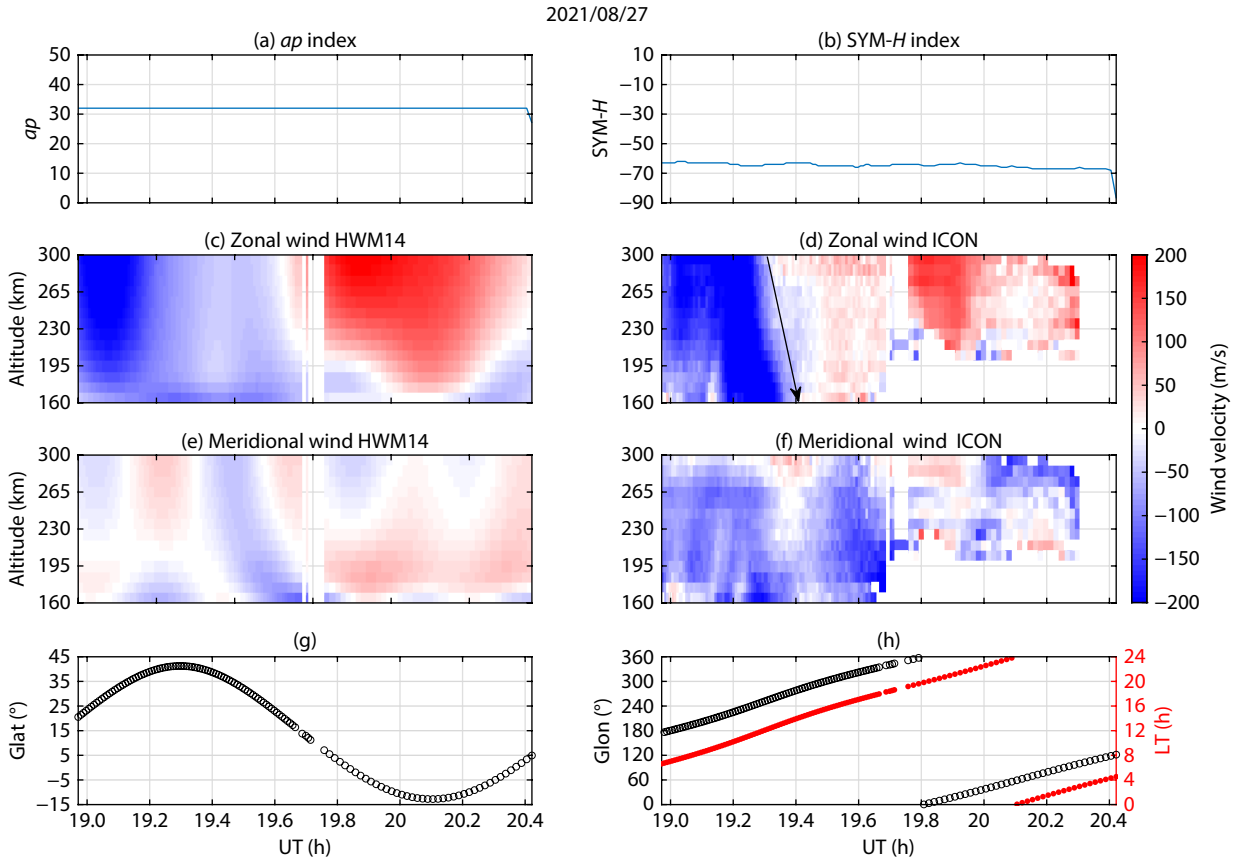

Figure 5. Same as Figure 4, but during the main phase of the storm. The arrow in panel (d) indicates the vertical shear of zonal wind in the main phase.

lower altitudes are southward. The response of the meridional winds on the dayside is not obvious, and in most of the regions where meridional winds exhibit a southward direction during the main phase of the storm, they return to the quiet time pattern, and the wind direction changes back to northward, like that before the storm. Similar to the results during the main phase period, the meridional winds estimated by HWM14 are much weaker.

Similar to Figure 5d, ICON observed that daytime zonal winds exhibit a clear vertical shear structure, as shown in Figure 6d; however, this vertical shear extends from lower altitudes toward higher altitudes. At 160 km around 4.6 UT (at 17°N Glat, 30°E Glon), the westward winds show amplitudes larger than 200 m/s, which are larger than the values at the other altitudes. The westward winds then gradually extend to 300 km around 4.8 UT (at 38°N Glat, 60°E Glon), and such an altitude shear structure is also not reproduced by HWM14. When looking at the development of the geomagnetic storm, this shear structure occurs by approximately 27 h after the SSC, with the SYM-*H* index recovering to the quiet-time pattern and the IMF B_z reaching approximately −5 nT.

4. Discussion

4.1 Characteristics of Winds from Both the ICON Observations and HWM Estimations During Geomagnetic Quiet Periods

Figures 1 and 2 show comparisons of neutral winds observed by ICON and estimated by HWM14 during geomagnetic quiet periods. The comparison provides us with a general understanding of the characteristics of neutral winds that change with the seasons, altitudes, and LTs. At the same time, our results can be considered an additional opportunity to evaluate the HWM14 estimations of the horizontal wind.

According to the ICON observations, the zonal winds are generally westward from 6:00 to 16:00 LT and eastward at the other LT hours at low latitudes and higher altitudes (Figures 1a and 1b). The westward winds in the middle latitude occur at 02:00 LT during the June solstice and at 04:00 LT during the December solstice. They then turn eastward at 15:00 LT (Figure 1c, right). At around sunrise hours, the westward winds generally appear at a later LT at a lower altitude. Similar vertical gradients of zonal winds exist at around 16:00 LT. Compared with the zonal winds, the change in meridional winds with the season, altitude, and latitude is much more pronounced. As shown in the ICON observations (Figures 2a and 2b), southward winds near the equatorial region dominate during the June solstice, and northward winds dominate during the December solstice. In the northern low latitudes, vertical reversals of the meridional winds are found at 08:00–12:00 LT from 300 to 160 km and at around 18:00 LT from 300 to 200 km during the June solstice. Similar reversals of the meridional winds are also found at around 06:00 LT from 300 to 160 km and around 00:00 LT from 270 to 200 km during the December solstice. In the southern low latitudes, meridional wind

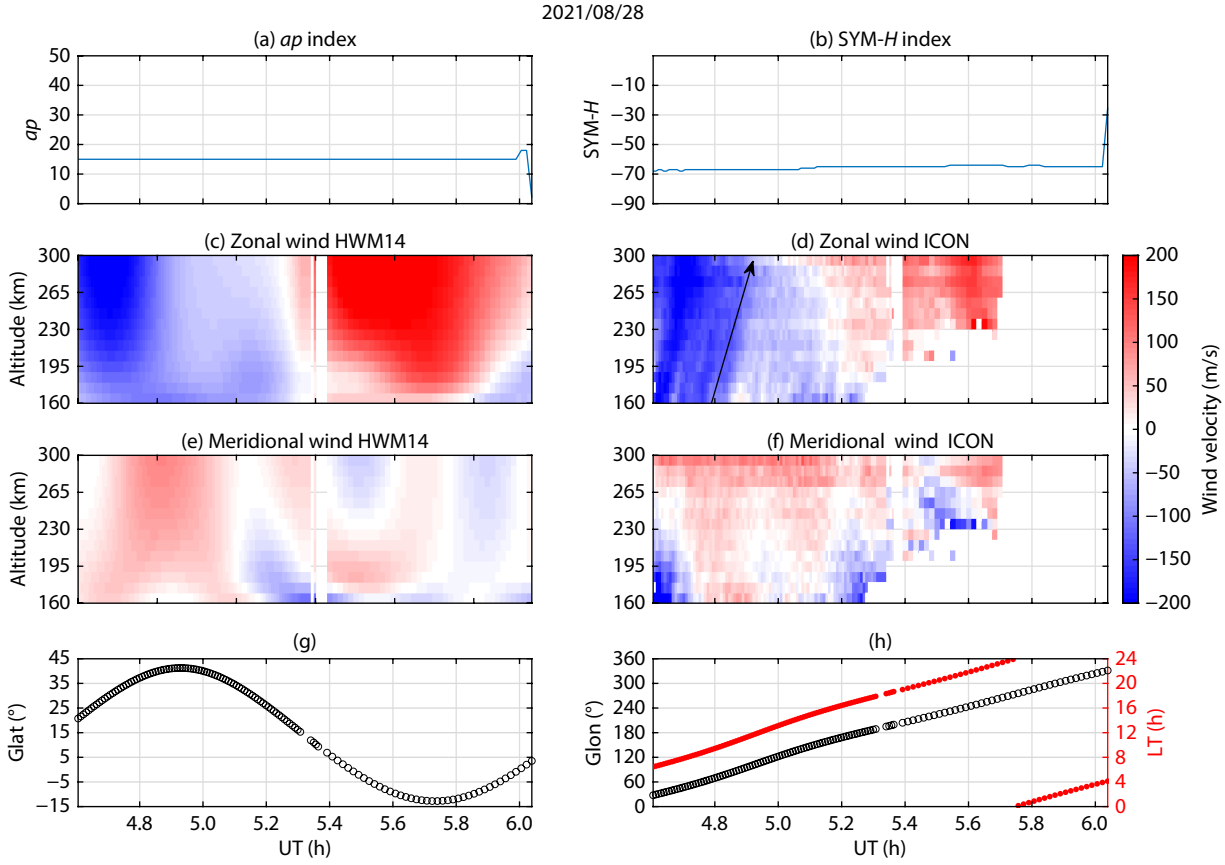

Figure 6. Same as Figure 4, but during the recovery phase. The arrow in panel (d) indicates the vertical shear of zonal wind in the recovery phase.

reversals occur at 08:00–12:00 LT below 200 km and at 21:00–02:00 LT from 300 to 200 km during the June solstice. During the December solstice, reversals of the meridional wind appear at 20:00–02:00 LT below 200 km and at 06:00–10:00 LT from 300 to 160 km during the December solstice. The meridional winds show almost opposite directions during the June and December solstices, and the meridional wind patterns during the equinox seasons are more like a transitional state between the June solstice and the December solstice. This result is in line with our expectations because the direction of meridional winds is closely related to the solar radiation heating in the two hemispheres, which shows the largest difference during the solstice months. In the northern middle latitudes, the patterns of meridional winds are markedly different from those near the equatorial regions. For example, the northward winds are dominant from 08:00 to 14:00 LT during the June solstice and from 06:00 to 20:00 LT during the December solstice, whereas the southward winds are dominant at the other times.

The horizontal wind estimations from HWM14 in most regions are similar to the ICON observations, especially in the middle latitudes. However, we also found differences between them. As shown in Figures 1a and 1b, the HWM14 estimations show that the westward winds are stronger in the morning at regions south of the equator, whereas in the afternoon hours, the same situations appear in regions north of the equator, but such a tendency can hardly be observed by ICON. We also noticed that in Figure 2b, ICON observed southward winds by around 06:00 LT in almost all seasons. These southward winds are usually short-lived and independent of the previous and subsequent northward winds, which led us to speculate that these southward winds might be caused by the different detection channels of MIGHTI on the dayside and nightside.

4.2 Vertical Gradient of Neutral Winds with Respect to the Development of the Geomagnetic Storm

Figures 4–6 show the neutral winds observed by ICON and estimated by HWM14 from typical orbits during the prestorm, main storm phase, and recovery phase from the storm on August 26–28, 2021, respectively. From the distributions of horizontal winds over UT versus altitude during the storm, we find that both the zonal and meridional winds during the active geomagnetic period are enhanced in the middle latitude more than at the low latitude. For meridional winds in the northern hemisphere, the disturbance winds during the geomagnetic storm are generally southward, which also means that the disturbance winds are equatorward. When a geomagnetic storm begins, the interaction between the solar wind and the magnetosphere intensifies the convection electric fields in the polar region, leading to a stronger ion movement along the electric fields. This large differential movement causes considerable Joule heating and ion drag, leading to the rapid expansion of the atmosphere and the significant enhancement of equatorial winds (e.g., Jee et al., 2008; Huang YS

et al., 2012).

Xiong C et al. (2015) pointed out that in the more active periods ($Kp > 4$), the disturbance winds in different latitude zones have different peak wind velocities. The middle latitude peak wind velocity is approximately 80 m/s, whereas the peak wind velocity at low latitudes is approximately 50 m/s. Unlike the findings of Xiong C et al. (2015), we explored the vertical gradients of neutral winds between 90 and 300 km on the dayside and nightside. We noticed that the meridional and zonal winds respond differently to storms at different altitudes and at different LTs. In comparison, on the dayside of the northern middle latitudes, during the main phase of the storm, a strong westward wind first appears at a higher altitude of approximately 300 km and then gradually extends to lower altitudes until 160 km, whereas in the recovery phase, the westward wind at lower altitudes first diminishes and then gradually develops to higher altitudes. For meridional winds at the same time and in the same region, the shape of the profile is opposite that of the zonal winds. During the main phase of the storm, a strong southward wind first appears at lower altitudes and then gradually extends to higher altitudes, whereas in the storm recovery phase, the southward wind at higher altitudes first weakens and then develops at lower altitudes. As mentioned in the previous paragraph, the enhancement of ion drift produces a strong ion drag and Joule heating, which leads to variations in the neutral winds. These processes are more effective at higher altitudes, and the effects of the storm propagate to the middle and lower latitudes. The inflow of energy from the higher elevations causes the zonal winds at higher altitudes (see Figure 5d) first to strengthen and then to extend to lower altitudes during the main phase. The different evolutions of zonal winds at different altitudes can cause the vertical shear, indicated by the arrow in Figure 5d. In the storm recovery phase, the energy inflow from the higher altitudes decreases, and the atmospheric heating from the storm causes the strong zonal winds at lower altitudes to extend to higher altitudes and form the vertical shear, indicated by the arrow in Figure 6d, unlike in the main phase of the storm.

In general, the difference between the neutral winds observed by ICON and estimated by HWM14 is larger during geomagnetic disturbed periods than during geomagnetic quiet periods, and ICON observed much more dramatic variations of the horizontal wind in the middle and upper atmosphere, when compared with the estimations from HWM14. However, note that because of the limited mission period of ICON, we have provided an analysis in this study during only one geomagnetic storm. Our intention is to highlight the fact that the horizontal neutral winds during the storm can exhibit distinct vertical gradients. To reach a more convincing conclusion, we encourage statistical analysis of horizontal winds during more geomagnetic storms.

5. Summary

In this study, we focused on the vertical gradient of horizontal neutral winds in the middle and upper atmosphere. Observations from the MIGHTI onboard the ICON satellite as well as estimations from HWM14 under the same conditions are also analyzed in detail. Our main findings are summarized as follows:

(1) During geomagnetic quiet periods, the estimations of both zonal and meridional winds from HWM14 show generally good agreement with the observations from ICON, in the altitude range of 160 to 300 km. According to observations near the equator, zonal winds reverse from westward to eastward at around 06:00 LT at higher altitudes, and the stronger westward winds preferentially appear at later LTs and lower altitudes. At around 16:00 LT, eastward winds reverse to westward, and vertical gradients of zonal winds similar to the sunrise hours can be observed. In the middle latitudes, zonal winds reverse approximately 2–4 h earlier than near the equator. Compared with zonal winds, the meridional wind varies more substantially with seasonal and latitudinal variations. Near the equator, according to the ICON observations, southward winds dominate during the June solstice, and northward winds dominate during the December solstice. In the northern low latitudes, vertical reversals of meridional winds are found at 08:00–13:00 LT from 300 to 160 km and at around 18:00 LT from 300 to 200 km during the June solstice. Similar reversals of meridional winds are also found at 04:00–07:00 LT from 300 to 160 km and at 22:00–02:00 LT from 270 to 200 km during the December solstice. In the southern low latitudes, meridional wind reversals occur at 08:00–11:00 LT from 200 to 160 km and at 21:00–02:00 LT from 300 to 200 km during the June solstice. During the December solstice, reversals of meridional winds appear at 20:00–01:00 LT below 200 km and at 06:00–11:00 LT from 300 to 160 km. In the northern middle latitudes, the northward winds are dominant from 08:00 to 14:00 LT at 230 km during the June solstice, and the northward winds persist until 16:00 LT at 160 and 300 km. During the December solstice, the northward winds are dominant from 06:00 to 21:00 LT, whereas the southward winds are dominant at the other times.

(2) The vertical variation in neutral winds during the geomagnetic storm on August 26–28, 2021, have been analyzed in detail. Both the meridional and zonal winds during the active geomagnetic period observed by ICON show distinguishable vertical shear structures at different stages of the storm. On the dayside, during the main phase of the storm, the peak velocities of the westward winds extend from higher altitudes to lower altitudes, whereas during the storm recovery phase, the peak velocities of the westward winds extend from lower altitudes to higher altitudes. The velocities of the southward winds are stronger at lower altitudes during the storm.

(3) The above-mentioned vertical structures of the horizontal winds during the storm could not be reproduced well by the HWM14 wind estimations. In addition, the overall response of the horizontal winds in the low and middle latitudes to the geomagnetic storm was underestimated by HWM14. The ICON observations provide a good dataset for improving the HWM14 wind estimations in the middle and upper atmosphere, especially the vertical variations.

Acknowledgments

This work was supported by the National Key R&D Program of China (Grant No. 2022YFF0503700) and the special funds of Hubei Luojia Laboratory (Grant No. 220100011). Chao Xiong was supported by the International Space Science Institute–Beijing (ISSI-BJ) project, “The Electromagnetic Data Validation and Scientific Application Research based on CSES Satellite” and ISSI/ISSI-BJ

project, "Multi-Scale Magnetosphere–Ionosphere–Thermosphere Interaction."

References

Antoniadis, D. A. (1976). Thermospheric winds and exospheric temperatures from incoherent scatter radar measurements in four seasons. *J. Atmos. Terr. Phys.*, *38*(2), 187–195. https://doi.org/10.1016/0021-9169(76)90127-6

Drob, D. P., Emmert, J. T., Meriwether, J. W., Makela, J. J., Doornbos, E., Conde, M., Hernandez, G., Noto, J., Zawdie, K. A., … Klenzing, J. H. (2015). An update to the horizontal wind model (HWM): The quiet time thermosphere. *Earth Space Sci.*, *2*(7), 301–319. https://doi.org/10.1002/2014EA000089

Emmert, J. T., Fejer, B. G., Fesen, C. G., Shepherd, G. G., and Solheim, B. H. (2001). Climatology of middle- and low-latitude daytime *F* region disturbance neutral winds measured by wind imaging interferometer (WINDII). *J. Geophys. Res.: Space Phys.*, *106*(A11), 24701–24712. https://doi.org/10.1029/2000JA000372

Englert, C. R., Babcock, D. D., and Harlander, J. M. (2007). Doppler asymmetric spatial heterodyne spectroscopy (DASH): Concept and experimental demonstration. *Appl. Opt.*, *46*(29), 7297–7307. https://doi.org/10.1364/ao.46.007297

Englert, C. R., Harlander, J. M., Brown, C. M., Marr, K. D., Miller, I. J., Stump, J. E., Hancock, J., Peterson, J. Q., Kumler, J., … Immel, T. J. (2017). Michelson interferometer for global high-resolution thermospheric imaging (MIGHTI): Instrument design and calibration. *Space Sci. Rev.*, *212*(1-2), 553–584. https://doi.org/10.1007/s11214-017-0358-4

Fesen, C. G. (1997). Geomagnetic activity effects on thermospheric tides: a compendium of theoretical predictions. *J. Atmos. Sol.-Terr. Phys.*, *59*(7), 785–803. https://doi.org/10.1016/S1364-6826(96)00106-X

Harding, B. J., Makela, J. J., Qin, J. Q., Fisher, D. J., Martinis, C. R., Noto, J., and Wrasse, C. M. (2017a). Atmospheric scattering effects on ground-based measurements of thermospheric vertical wind, horizontal wind, and temperature. *J. Geophys. Res.: Space Phys.*, *122*(7), 7654–7669. https://doi.org/10.1002/2017JA02394

Harding, B. J., Makela, J. J., Englert, C. R., Marr, K. D., Harlander, J. M., England, S. L., and Immel, T. J. (2017b). The MIGHTI wind retrieval algorithm: description and verification. *Space Sci. Rev.*, *212*(1-2), 585–600. https://doi.org/10.1007/s11214-017-0359-3

Harding, B. J., Chau, J. L., He, M. S., Englert, C. R., Harlander, J. M., Marr, K. D., Makela, J. J., Clahsen, M., Li, G. Z., … Immel, T. J. (2021). Validation of ICON-MIGHTI thermospheric wind observations: 2. Green-line comparisons to specular meteor radars. *J. Geophys. Res.: Space Phys.*, *126*(3), e2020JA028947. https://doi.org/10.1029/2020JA028947

Heelis, R. A. (2004). Electrodynamics in the low and middle latitude ionosphere: A tutorial. *J. Atmos. Sol.-Terr. Phys.*, *66*(10), 825–838. https://doi.org/10.1016/j.jastp.2004.01.034

Huang, Y. S., Richmond, A. D., Deng, Y., and Roble, R. (2012). Height distribution of Joule heating and its influence on the thermosphere. *J. Geophys. Res.: Space Phys.*, *117*(A8), A08334. https://doi.org/10.1029/2012JA017885

Huang, Y. Y., Xiong, C., Wu, J. W., Stolle, C., Wang, F. J., Zheng, Y. H., Xu, C. Y., Hu, Y., and Wang, S. M. (2023). Dayside vertical wind reversal at transition altitude from E to F regions observed by the ICON satellite. *Earth Space Sci.*, *10*(5), e2023EA002836. https://doi.org/10.1029/2023EA002836

Immel, T. J., Harding, B. J., Heelis, R. A., Maute, A., Forbes, J. M., England, S. L., Mende, S. B., Englert, C.R., Stoneback, R. A., ... Makela, J. J. (2021). Regulation of ionospheric plasma velocities by thermospheric winds. *Nat. Geosci., 14*, 893–898. https://doi.org/10.1038/s41561-021-00848-4

Jee, G., Burns, A. G., Wang, W., Solomon, S. C., Schunk, R. W., Scherliess, L., Thompson, D. C., Sojka, J. J., and Zhu, L. (2008). Driving the TING model with GAIM electron densities: Ionospheric effects on the thermosphere. *J. Geophys. Res.: Space Phys.*, *113*(A3), A03305. https://doi.org/10.1029/2007JA012580

Lieberman, R. S., Akmaev, R. A., Fuller–Rowell, T. J., and Doornbos, E. (2013). Thermospheric zonal mean winds and tides revealed by CHAMP. *Geophys. Res. Lett.*, *40*(10), 2439–2443. https://doi.org/10.1002/grl.50481

Liu, H. X., Lühr, H., Watanabe, S., Köhler, W., Henize, V., and Visser, P. (2006). Zonal winds in the equatorial upper thermosphere: Decomposing the solar flux, geomagnetic activity, and seasonal dependencies. *J. Geophys. Res.: Space Phys.*, *111*(A7), A07307. https://doi.org/10.1029/2005JA011415

Makela, J. J., Baughman, M., Navarro, L. A., Harding, B. J., Englert, C. R., Harlander, J. M., Marr, K. D., Benkhaldoun, Z., Kaab, M., and Immel, T. J. (2021). Validation of ICON-MIGHTI thermo-spheric wind observations: 1. Nighttime red-line ground-based Fabry–Perot interferometers. *J. Geophys. Res.: Space Phys.*, *126*(2), e2020JA028726. https://doi.org/10.1029/2020JA028726

McGinness, E. C., Immel, T. J., Harding, B. J., Wu, Y. J., and Triplett, C. C. (2023). The effects of a small geomagnetic storm on Earth's thermosphere and ionosphere: ICON observations of the 25 January 2021 disturbance. *J. Geophys. Res.: Space Phys.*, *128*(7), e2022JA031207. https://doi.org/10.1029/2022JA031207

McLandress, C., Rochon, Y., Shepherd, G. G., Solheim, B. H., Thuillier, G., and Vial, F. (1994). The meridional wind component of the thermospheric tide observed by WINDII on UARS. *Geophys. Res. Lett.*, *21*(22), 2417–2420. https://doi.org/10.1029/94GL02367

Richmond, A. D., Peymirat, C., and Roble, R. G. (2003). Long-lasting disturbances in the equatorial ionospheric electric field simulated with a coupled magnetosphere-ionosphere-thermosphere model. *J. Geophys. Res.: Space Phys.*, *108*(A3), 1118. https://doi.org/10.1029/2002JA009758

Richmond, A. D. (2011). Electrodynamics of ionosphere-thermosphere coupling. In M. A. Abdu, et al. (Eds.), *Aeronomy of the Earth's Atmosphere and Ionosphere* (pp. 191–201). Dordrecht, the Netherlands: Springer. https://doi.org/10.1007/978-94-007-0326-1_13

Wang, W., Burns, A. G., Wiltberger, M., Solomon, S. C., and Killeen, T. L. (2008). Altitude variations of the horizontal thermospheric winds during geomagnetic storms. *J. Geophys. Res.: Space Phys.*, *113*(A2), A02301. https://doi.org/10.1029/2007JA012374

Xiong, C., Lühr, H., and Fejer, B. G. (2015). Global features of the disturbance winds during storm time deduced from CHAMP observations. *J. Geophys. Res.: Space Phys.*, *120*(6), 5137–5150. https://doi.org/10.1002/2015JA021302

Xiong, C., Lühr, H., and Fejer, B. G. (2016). The response of equatorial electrojet, vertical plasma drift, and thermospheric zonal wind to enhanced solar wind input. *J. Geophys. Res.: Space Phys.*, *121*(6), 5653–5663. https://doi.org/10.1002/2015JA022133